3-1-2022

A gyroscope-based system for intraoperative measurement of tibia coronal plane alignment in total knee arthroplasty

Michael A. Kokko
Thayer School of Engineering at Dartmouth

Ryan M. Chapman
Thayer School of Engineering at Dartmouth

Martin W. Roche
Holy Cross Hospital, Fort Lauderdale

Douglas W. Van Citters
Thayer School of Engineering at Dartmouth

Medicine in Novel Technology and Devices 13 (2022) 100112

Contents lists available at ScienceDirect

Medicine in Novel Technology and Devices

journal homepage: www.journals.elsevier.com/medicine-in-novel-technology-and-devices/

Full Length Article

A gyroscope-based system for intraoperative measurement of tibia coronal plane alignment in total knee arthroplasty

Michael A. Kokko [a,*], Ryan M. Chapman [a,b], Martin W. Roche [c], Douglas W. Van Citters [a]

[a] Thayer School of Engineering at Dartmouth College, 14 Engineering Drive, Hanover, NH, 03755, USA
[b] Department of Kinesiology, College of Health Sciences, University of Rhode Island, 25 W. Independence Way, Kingston, RI, 02881, USA
[c] Orthopedic Research Institute Holy Cross Hospital, 4725 N Federal Hwy.Ft, Lauderdale, FL, 33308, USA

ARTICLE INFO

Keywords:
Alignment
Gyroscope
Inertial measurement unit
Inertial sensing
Orthopedic procedures
Prosthetics
Total knee arthroplasty

ABSTRACT

Coronal plane alignment in total knee arthroplasty (TKA) is an important predictor of clinical outcomes including patient satisfaction and device longevity. Radiography and computer assisted navigation are the two primary technologies currently available to surgeons for intraoperative assessment of alignment; however, neither is particularly well-suited for use in this increasingly high volume procedure. Herein we propose a novel gyroscope-based instrument for intraoperative validation of tibia coronal plane alignment, and provide initial analytical and experimental performance assessments. The gyroscope-based alignment estimate is derived from simplified joint geometry and verified experimentally using a custom tibial trial insert containing a consumer-grade inertial measurement unit (IMU). Average accuracy of the gyroscope-based tibia coronal angle estimate was found to be within ±1° in mechanical leg jig and cadaver testing. These results indicate that the proposed gyroscope-based method shows promise for low cost, accurate intraoperative validation of limb alignment in TKA patients. Integrating IMU technology into the TKA surgical workflow via low-cost instrumentation will enable surgeons to easily validate implant alignment in real time, thereby reducing cost, operating room time, and future revision burden.

1. Introduction

Total joint arthroplasty (TJA) is one of the most effective medical interventions of the modern age; its high rates of patient satisfaction reflecting the degree to which knee and hip prostheses have enabled aging populations to overcome the debilitating pain associated with osteoarthritis [1–5]. Total knee arthroplasty (TKA) alone is among the most commonly performed surgical procedures in the United States with over 750,000 cases logged each year, and 1–2 million expected annually by 2030 [6–8]. While patients undergoing TKA generally report satisfaction with their prostheses, the high case volume underscores the importance of minimizing complications, and by extension, the need for costly revision surgeries. With 200,000 TKA revisions expected annually by 2030, improved accuracy in placing primary components may reduce the TKA revision burden as malalignment is known to exacerbate many of the conditions for which revision is indicated [2–5,9,10].

Surgeons have historically aimed to achieve neutral post-operative *mechanical* alignment of the lower extremity (i.e. planar resections made normal to the hip-knee axis on the femur, and the knee-ankle axis on the tibia as shown in Fig. 1), employing a variety of techniques including preoperative radiography and intramedullary or extramedullary guides to ensure a natural distribution of load across the condyles [11–15]. Much of the orthopedic literature supports mechanical alignment where resections are made within ±3° of the appropriate neutral axes (most critically in the coronal plane) [16]. Recent attempts to further improve patient outcomes have centered on *kinematic* alignment, in which the articulation of the postoperative knee is tuned to closely match that of each patient's pre-arthritic anatomy [11,12,15]. While much effort has been directed toward rectifying the various approaches to TKA alignment [11,12,14–21], in all cases surgeons are concerned with the angular accuracy of the distal femur and proximal tibia resections.

Several resection planning and validation tools are currently available, each with its own advantages and limitations [22–27]. At the most basic level, surgical cutting jigs can be configured to guide a bone saw to produce a planar resection surface on either the distal femur or the

* Corresponding author.
E-mail addresses: Michael.Kokko@dartmouth.edu (M.A. Kokko), rmchapman@uri.edu (R.M. Chapman), martin@mroche.com (M.W. Roche), Douglas.W.Van.Citters@dartmouth.edu (D.W. Van Citters).

https://doi.org/10.1016/j.medntd.2021.100112
Received 28 July 2021; Received in revised form 19 December 2021; Accepted 27 December 2021

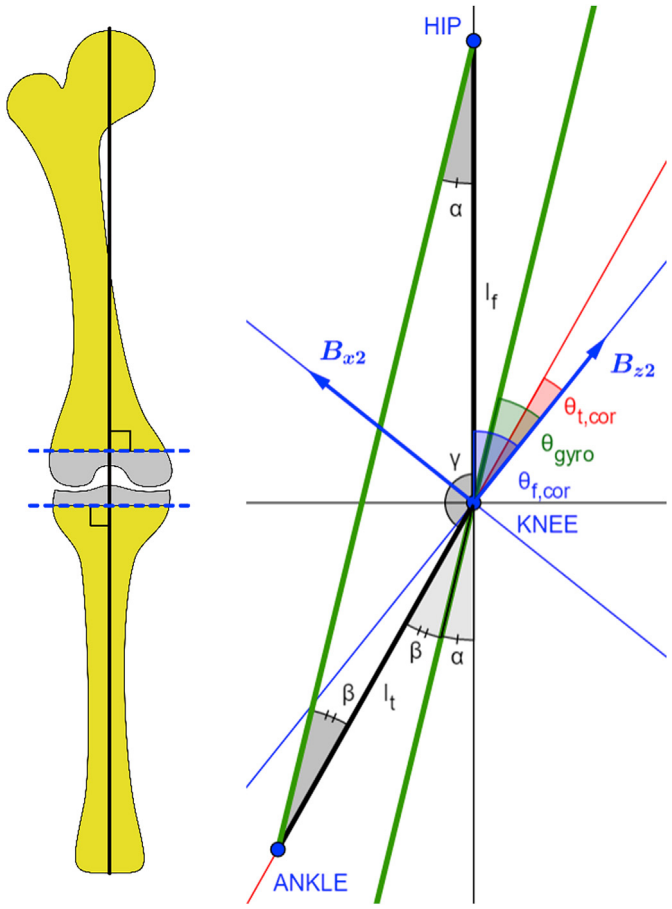

Fig. 1. Left: Lower extremity in neutral mechanical alignment ($\theta_{f,cor} = \theta_{t,cor} = 0$) with the distal femur and proximal tibia resections (dashed lines) taken in the transverse plane normal to the mechanical axis of the leg (solid line). Right: Coronal leg geometry from which (1) is derived. The IMU device is aligned with the B_{xyz2} coordinate system. This model assumes neutral alignment in the sagittal plane and no transverse rotation of the tibial component. The black lines of lengths ℓ_f and ℓ_t represent the *mechanical* (rather than anatomical) axes of the femur and tibia.

proximal tibia whose orientation in space is fully specified with respect to the three standard anatomical planes (sagittal, coronal, and transverse). When indicated, resections made by this method can be validated by intraoperative plain radiography or fluoroscopy; however, these methods add additional time and cost to the procedure, and expose both the patient and the surgical team to ionizing radiation. Moreover, these traditional methods are relatively inaccurate. Teter et al. showed that while 92% of resections made via an extramedullary cutting system fall within ±4° of the target coronal angle, they fail to achieve the widely accepted target of ±3° [16,23]. As a result, some surgeons have turned to optical (e.g. infrared) or electromagnetic (e.g. radio frequency) navigation to achieve accuracy better than ±1° [28]. Increased operating room (OR) time for registration and planning as well as high capital costs are, however, distinct barriers to widespread adoption [22,24–27,29–37]. Robot-assisted knee surgery also provides an opportunity for both specifying and validating resection plane orientation, offering tibial alignment accuracy on the order of ±1°, but like tracked navigation requiring significant capital investment and imposing a learning curve on OR time [38–40].

Orthopedic device manufacturers have recently begun to introduce the next generation of surgical resection planning and validation tools based on strapdown inertial measurement units (IMUs) which have long been used for nonsurgical measurement of human joint kinematics [41–44]. Intraoperatively, these new devices collect data from micro-electromechanical systems (MEMS) sensors – typically accelerometers – to identify the orientation of surgical resection planes. Although such devices have demonstrated accuracy to ±2° or ±3° while decreasing procedure lengths compared to traditional computer navigation, the hardware can be cumbersome and the accelerometer-based commercial systems often require rapid or jerky intraoperative manipulations of the leg about the hip joint to achieve sufficiently high linear acceleration for analysis at the knee [45–52]. Thus, there remains a distinct need within the orthopedic community for efficient, cost effective, user-friendly, and analytically sound methods of quantifying intraoperative TKA alignment.

This work develops a geometric foundation for gyroscope-based assessment of tibial coronal plane alignment, setting the stage for a similarly-implemented multiplane alignment system. The proposed method and evaluation techniques are outlined in Section 2, with a derivation from first principles and a more complete model for error analysis presented in Section 3. Section 4 reviews preliminary experimental results obtained using the prototype device in simulation, with a mechanical leg jig, and with a cadaver model. A discussion of the observed results and future applications follows in Section 5, with a conclusion in Section 6.

2. Materials and methods

The proposed method for validating tibial alignment requires temporarily installing a specialized trial bearing instrumented with a MEMS rate gyroscope on the tibial tray in place of the final polyethylene component. While elevating the leg comfortably (e.g. 30°) above the surgical table, the surgeon performs a series of internal/external rotations about the hip-ankle axis (Fig. 2). This maneuver need not be jerky; even small rotations of amplitude 15–20° at approximately 1 Hz produce reasonable angular velocity streams ω_x and ω_z from which the tibia coronal angle can be calculated as

$$\widehat{\theta}_{t,cor} = \tan^{-1}\left(\frac{\omega_x}{\omega_z}\right) - \sin^{-1}\left(\frac{\ell_f}{\ell_t}\sin\left(\theta_{f,cor} - \tan^{-1}\left(\frac{\omega_x}{\omega_z}\right)\right)\right) \quad (1)$$

where ω_x and ω_z are the components x and z components of angular velocity, ℓ_f and ℓ_t are the lengths of the femur and tibia, and $\theta_{f,cor}$ is the coronal angle of the distal femur resection plane. This equation is derived from a simplified planar model of the lower extremity and described in more detail in Section 3.1.

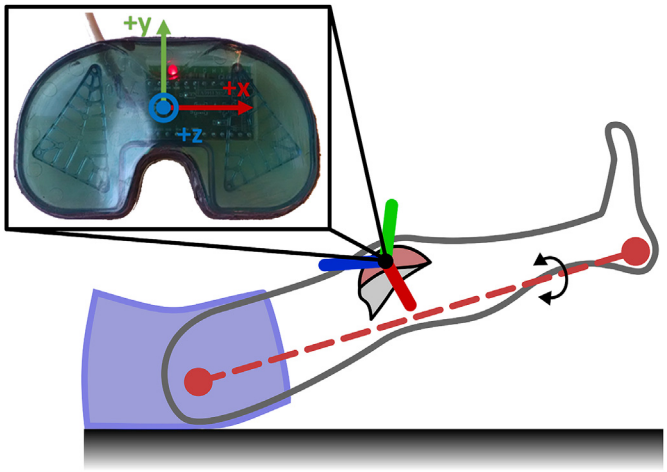

Fig. 2. A prototype OrthoSensor VERASENSE™ tibial trial housing is shown outfitted with an ST LSM6DS3 IMU evaluation board. With the instrumented trial temporarily placed in the joint, the leg is elevated and gently rotated about the hip-ankle axis. Coronal alignment of the proximal tibia resection plane is estimated from gyroscope output.

2.1. In silico planar sensitivity analysis

Of the five parameters included in (1), ω_x and ω_z are obtained directly from the IMU, ℓ_f and ℓ_t must be measured by the surgical team or estimated from imaging, and $\theta_{f,cor}$ is assumed to be known or measured separately. To assess the sensitivity of $\widehat{\theta}_{t,cor}$ to perturbations (e.g. measurement error) in each of these five parameters, a linear approximation of (1) was obtained by computing partial derivatives and evaluating each about a nominal operating point. The absolute expected contribution to overall error associated with each parameter was computed from the product of the partial derivative and the expected maximum parameter deviation. We assumed reasonable deviations based on typical gyroscope nonlinearity ($\Delta\omega_x = \Delta\omega_y = 1^\circ/\text{s}$), manual measurements of bone lengths between anatomical landmarks ($\Delta\ell_f = \Delta\ell_t = 1\text{cm}$), and the expected accuracy of the femur coronal cut ($\Delta\theta_{f,cor} = 2^\circ$) [53].

Using nominal parameter values consistent with our benchtop mechanical leg model, we estimated an upper bound for the instantaneous absolute error in (1) given a sinusoidal leg rotation of amplitude $120^\circ/\text{s}$ and frequency 1 Hz as observed during cadaver experimentation. This analysis informed our choice of method for computing $\tan^{-1}\left(\frac{\omega_x}{\omega_z}\right)$ during benchtop and cadaver evaluations.

2.2. In silico 3D sensitivity analysis

In addition to examining the effects of sensor noise and other measurement errors on the $\widehat{\theta}_{t,cor}$ estimate in (1), it is also important to understand the expected error contributions from sagittal and transverse plane angular misalignment, as well as from joint flexion or flexion contracture. We therefore constructed a more complete geometrical model of the relevant anatomy, detailed in Section 3.2, which relates a known limb state to the expected gyroscope output and $\widehat{\theta}_{t,cor}$ estimate. The forward model was evaluated across a clinically-relevant range of joint states: $\pm10^\circ$ tibial coronal and sagittal angles, $\pm5^\circ$ tibial component transverse misalignment, $\pm15^\circ$ residual flexion/extension, and 0–250 mm articulation radius yielded a set of sensitivity maps detailing the effects of modeling error associated with the planar geometry assumption implicit in (1), as well as the effect of parasitic knee articulation or flexion contracture, on the estimated tibia coronal alignment $\widehat{\theta}_{t,cor}$.

2.3. Experimental data collection system

Four prototypes of the proposed instrumented tibial trial (Fig. 2) were fabricated from VERASENSE™ housings (OrthoSensor Inc., Dania Beach, FL) and ST LSM6DS3 IMU development boards (ST Microelectronics, Geneva, Switzerland). Angular rate data from each device were captured using an ATxmega256A3BU microcontroller (Atmel Corporation, San Jose, CA) running at 16 MHz via a tethered SPI connection. Gyroscope output was recorded at 100 Hz, timestamped by the microcontroller upon collection, then passed via RS232 to a laptop and processed through a series of custom MATLAB scripts (MathWorks, Natick, MA). Each prototype device was calibrated to correct for variations in sensitivity and misalignment of gyroscope axes within the VERASENSE™ housing using a purpose-built rotational fixture with synchronized optical encoder output.

2.4. In vitro leg jig evaluation

Laboratory assessment of the gyroscope-based tibia coronal plane alignment procedure described in Section 2 was performed using a mechanical "leg jig" model of knee arthroplasty as shown in Fig. 3. This simulated left leg comprises a ball and socket hip joint, a TKA femoral component, aluminum femur and tibia rods, and graduated, lockable articulation points for adjusting the femur and tibia coronal angles. The joint line rotation maneuver was performed repeatedly (ten trials per configuration) with the prototype device installed between the femur and tibia, for tibia coronal angles between -4.4° (varus) and $+4.4^\circ$ (valgus). Rotations were first performed with fixed hip and ankle pivot points to constrain motion to the desired axis, and then again with the leg elevated at roughly 30° as would be expected in the OR.

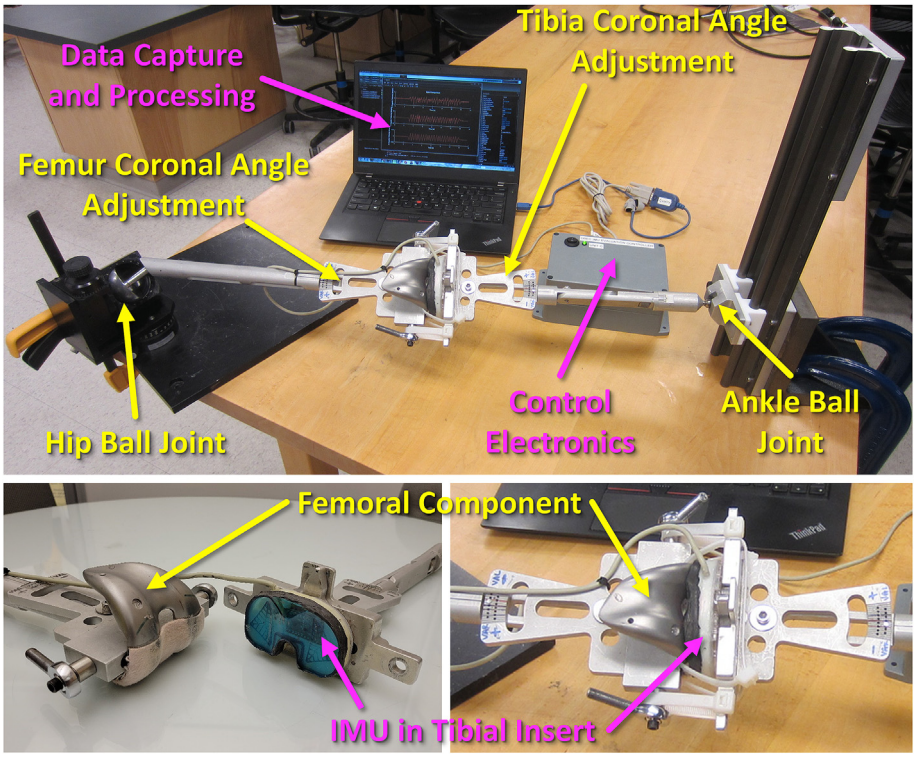

Fig. 3. Experimental setup for bench-top assessment of the proposed tibia coronal angle estimation procedure.

In all testing, the knee joint was compressed with cable ties to prevent parasitic rotation of the instrumentation, and the femur coronal angle was held constant at +1° varus (measured using digital photography). The true tibia coronal angle $\theta_{t,cor}$ is reported as the leg jig tibia setting scaled by a factor of 0.88 which accounts for the 4.25 cm offset between the pivot point of the coronal adjustment and the knee joint.

2.5. Ex vivo cadaver evaluation

Accuracy of the gyroscope-based tibia alignment estimate was also assessed with the prototype instrumented trial placed in the left leg of a 51-year-old cadaveric specimen with no known or observed orthopedic abnormalities. A board-certified orthopedic surgeon prepared the specimen following standard TKA protocol, then inserted the prototype device on the tibial tray in place of the polyethylene bearing (Fig. 4). Throughout testing the femur was maintained at -2° (valgus) in the coronal plane and +2° (flexion) in the sagittal plane. The tibia was cut progressively from -2° (varus) through 0° (neutral) to +2° (valgus) in the coronal plane. The surgeon and an assistant with significant orthopedic experience each performed 2–3 trials of the joint line rotation maneuver in every configuration, and the tibia coronal angle computed based on gyroscope output was compared against ground truth measurements made with an optically-tracked Stryker TKA navigation system (Stryker Corporation, Kalamazoo, MI).

3. Calculation

In this section we first develop (1) directly from simplified coronal plane geometry, and then construct a three dimensional forward model to analyze the effects of sagittal and transverse plane misalignment. Sign conventions with respect to distal femur and proximal tibia angles are chosen as shown in Fig. 5 following the widely accepted work of Grood and Suntay [54]. Unless otherwise stated, reference frames placed are taken to be right handed and oriented with the x axis directed toward the patient's right side, y toward the anterior, and z toward the superior (often toward the hip).

3.1. Proposed tibia coronal plane angle estimate

The geometry of a lower extremity (either left or right) is illustrated in Fig. 1 under the important assumption that all misalignment occurs in the coronal plane, the validity of which is addressed in Section 3.2. The distal femur is taken to be cut as a plane such that its normal vector forms an angle $\theta_{f,cor}$ with the mechanical axis of the femur. Likewise, the vector normal to the proximal tibia resection plane forms an angle $\theta_{t,cor}$ with the mechanical axis of the tibia.

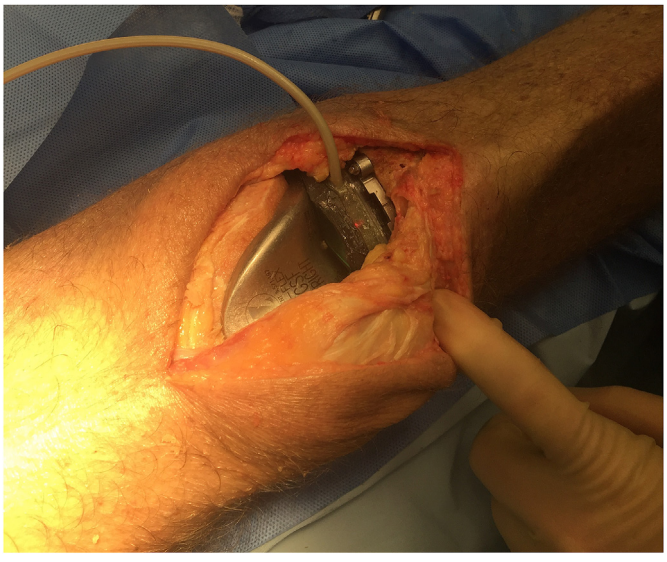

Fig. 4. Experimental setup for cadaver model assessment of the proposed tibia coronal angle estimation procedure.

Since the angular velocity vector associated with the prescribed internal/external rotation maneuver lies parallel to the joint line (hip-ankle axis), the angle between the joint line and the IMU z axis is given by:

$$\theta_{gyro} = \tan^{-1}\left(\frac{\omega_x}{\omega_z}\right) \tag{2}$$

where ω_x and ω_z are the IMU-reported angular velocities about the gyroscope x and z axes, respectively. Examination of the simplified lower extremity geometry presented in Fig. 1 gives $\theta_{t,cor} = \theta_{gyro} - \beta$. Solving for β using the law of sines yields a direct expression for the tibia coronal angle:

$$\theta_{t,cor} = \theta_{gyro} - \sin^{-1}\left(\frac{\ell_f}{\ell_t}\sin\left(\theta_{f,cor} - \theta_{gyro}\right)\right) \tag{3}$$

Combining (2) and (3) produces (1) which expresses the tibial coronal alignment estimate $\widehat{\theta}_{t,cor}$ in terms of gyroscope measurements ω_x and ω_z.

3.2. Forward measurement model

The femoral side of the forward model starts with a neutral distal femur represented by a rectangular prism extending from the hip (O_{xyz}) in the direction of the femur mechanical axis (Fig. 6, left). Once cut, the orientation of the resection plane can be described in terms of two angles: $\theta_{f,cor}$, the angle formed between the femur mediolateral axis and its projection on the resection plane; and $\theta_{f,sag}$, the angle formed between the femur anteroposterior axis and its projection. Although the two vectors that represent these axis projections are not necessarily orthogonal, they do form a basis for the resection plane and their cross product identifies its normal direction.

Taking the resection plane normal as $\boldsymbol{A}_{z0}$ (Fig. 6), a right-handed coordinate system A_{xyz0} is established by placing orthogonal vectors $\boldsymbol{A}_{x0}$ and $\boldsymbol{A}_{y0}$ in the resection plane such that $\boldsymbol{A}_{y0}$ also lies within the femur sagittal plane. The A_{xyz} coordinate frame is then defined by rotating A_{xyz0} by $\theta_{f,trans}$ about $\boldsymbol{A}_z = \boldsymbol{A}_{z0}$ to simulate rotational misalignment of the femoral component. Finally, a convex, semi-cylindrical articular surface with radius r_{artic} is affixed to A_{xyz} such that the cylinder axis is parallel to $\boldsymbol{A}_x$. This procedure fully determines the orientation of A_{xyz}, and its position in space is given by a displacement ℓ_f in the $-O_z$ direction from the origin of the O_{xyz} (hip) frame. Although in practice resection of the distal femur typically requires multiple oblique cuts, the pose of the femoral component is sufficiently described by this planar approximation.

The tibial side of the forward model proceeds identically to the femoral development up to the point of establishing B_{xyz} on the proximal tibia resection plane (Fig. 6, right). Note that the ankle is known to be at a distance ℓ_t along the tibia mechanical axis from the center of the resected surface, so its position can be expressed in B_{xyz} by a simple rigid transformation. A *concave* articular surface, otherwise equivalent to that applied to the femur, is attached to B_{xyz}, then the two articular surfaces are aligned such that B_{xyz} coincides with A_{xyz}. At this stage B_{xyz} is relabeled B_{xyz1} for clarity.

As illustrated in Fig. 7, we next rotate the tibia model about the mated cylindrical surface (i.e. articulate the knee) by an angle θ_{artic} that makes the line from the origin of the B frame to the ankle (tibia mechanical axis) parallel to the $O_x - O_z$ (femur coronal) plane. The B frame is again relabeled B_{xyz2} at this stage as it now represents the pose of the IMU during the intraoperative joint line rotation maneuver.

The final step in construction of the forward model is expressing the joint line vector (O_{xyz} to ankle) in the sensor B_{xyz2} frame. The ratio of the joint line component along $\boldsymbol{B}_{x2}$ to that along $\boldsymbol{B}_{z2}$ replaces the argument of the arctangent term in (2) which, when combined with (3), yields the

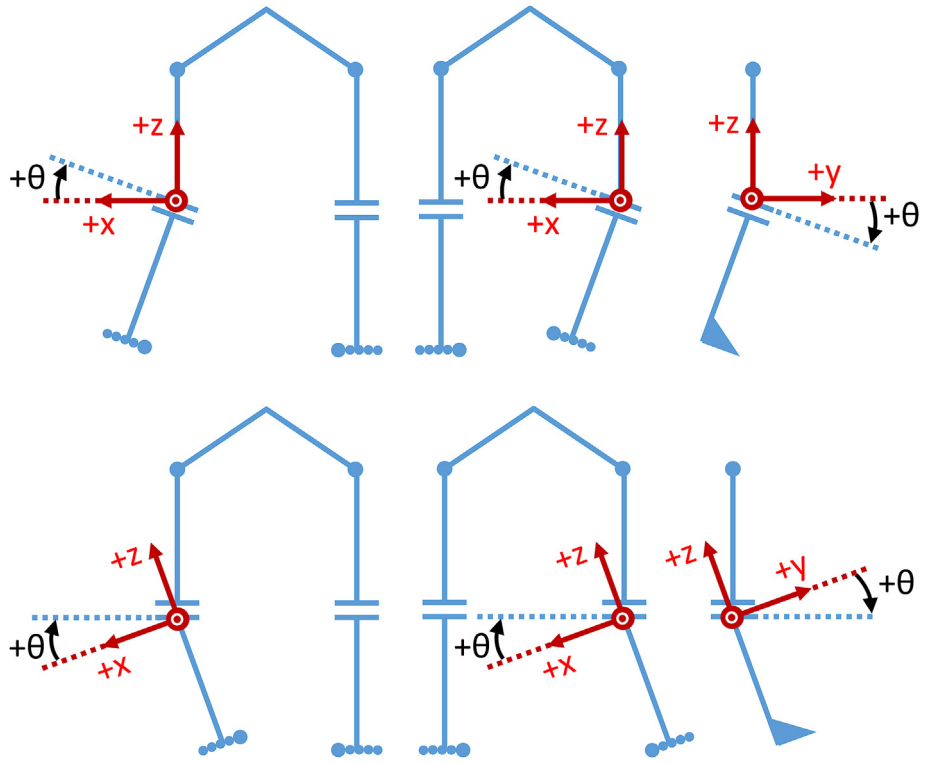

Fig. 5. Sign conventions used for referencing the coronal and sagittal orientation of resection planes on the distal femur (top row) and proximal tibia (bottom row) are chosen for consistency with Grood and Suntay [54]. The neutral state ($\theta = 0^\circ$ for each cut) reflects mechanical alignment.

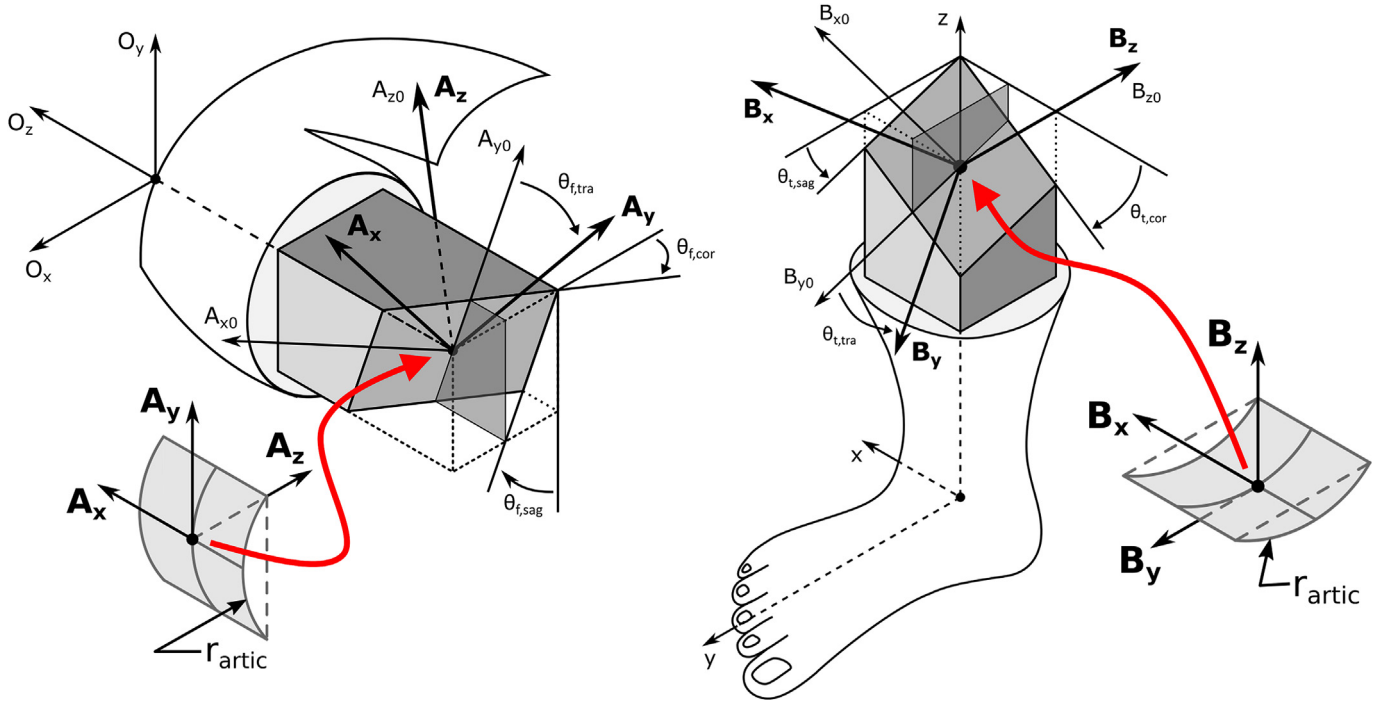

Fig. 6. The distal femur (left) and proximal tibia (right) cuts are each modeled as planar resections measured with respect to the nominal mediolateral and anteroposterior axes as $\theta_{.cor}$ and $\theta_{.sag}$, respectively. The inferosuperior axis (z axis) in each case is the *mechanical* axis of the respective long bone. Each reference coordinate system may be rotated by some transverse angle $\theta_{.tra}$ defined between its y axis and the sagittal plane. Semi-cylindrical patches model the convex femoral head and concave bearing articular surfaces and are aligned with the femur and tibia as illustrated.

expected estimate of $\widehat{\theta}_{t,cor}$ from (1) given the coronal, sagittal, and transverse angles, long bone lengths, and articulation radius from which the model was constructed. The expected error in the tibia coronal angle estimate is calculated as the difference between $\widehat{\theta}_{t,cor}$ and the value of $\theta_{t,cor}$ specified in construction of the forward model.

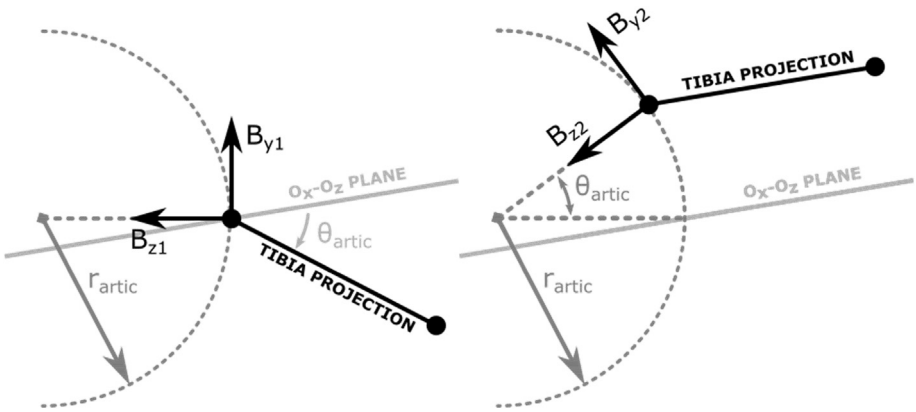

Fig. 7. The A_{xyz} and B_{xyz} coordinate systems at the distal femur and proximal tibia are aligned, mating the two semi-cylindrical surfaces (left). The tibia model is then articulated about the sole degree of freedom by θ_{artic} until the mechanical axis of the tibia lies parallel to the O_x-O_z (femur coronal) plane (right).

4. Experimental testing and results

4.1. Planar sensitivity analysis

Simulated sinusoidal leg rotations (Fig. 8) reveal the time evolution of the error contributed to $\widehat{\theta}_{t,cor}$ by variations in each of the parameters of (1). The sum of absolute error (SAE) metric serves as a "worst case" upper bound on noise-related error in $\widehat{\theta}_{t,cor}$, and is minimized to 3.55° at mid-rotation as angular speed peaks. The accuracy of the proposed procedure is largely driven by the accuracy of the femur coronal angle measurement, whose variations translate almost directly into tibia coronal angle error $\left(\left|\frac{\partial\widehat{\theta}_{t,cor}}{\partial\theta_{f,cor}}\right| = 1.17\right)$ for the assumed geometry. Erroneous bone length measurements, on the other hand, are much less consequential $\left(\left|\frac{\partial\widehat{\theta}_{t,cor}}{\partial\ell_f}\right| = 0.10,\ \left|\frac{\partial\widehat{\theta}_{t,cor}}{\partial\ell_t}\right| = 0.12\right)$. The peaks in SAE at low angular speed are driven by gyroscope noise, and could in theory be avoided by estimating $\widehat{\theta}_{t,cor}$ only when the magnitude of angular velocity exceeds some threshold. In benchtop and cadaver testing, rather than computing (1) in a pointwise fashion and discarding low speed data, we computed the argument of the arctangent term in (2) as the slope of a regression line between ω_x and ω_z for all maneuver data where ω_x is the dependent and ω_z the independent variable. Low speed gyroscope errors have relatively little effect on this regression due to the symmetric nature of the maneuver, and a single value of $\widehat{\theta}_{t,cor}$ is returned irrespective of the number of oscillations performed.

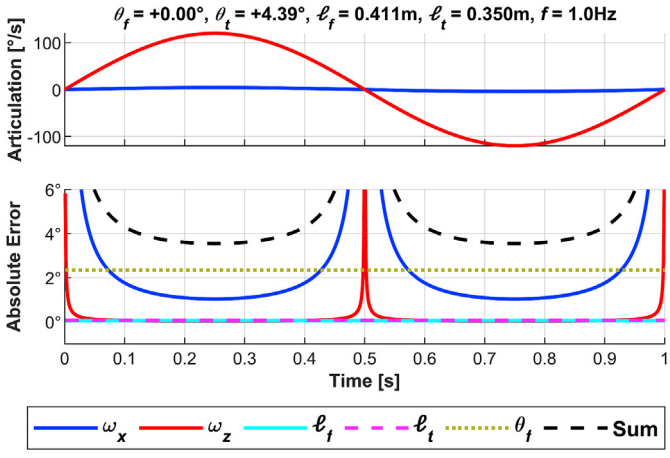

Fig. 8. A simulated joint line rotational trajectory (top) approximates measured motion profiles from cadaver experimentation to estimate the phase-dependency of error propagation through the proposed tibial coronal angle calculation (bottom). The distal femur cut was taken to be normal to its mechanical axis, and the tibia cut at 4.39° for consistency with the maximum leg jig settings. A perturbation of 1°/s was applied to gyroscope readings, 1cm to bone lengths, and 2° to the femur coronal angle. The upper bound of maximum absolute error in the estimated tibia coronal angle (black dashed line) was minimized to 3.55° when the magnitude of the articulation rate peaked at mid swing. The most significant error component at mid swing was associated with the estimated femur coronal angle, while bone length perturbations had no significant effect on the calculation.

4.2. 3D sensitivity analysis

Fig. 9 illustrates how clinically relevant coronal, sagittal, and transverse angular misalignments of the tibial tray translate into error in $\widehat{\theta}_{t,cor}$. Again assuming a 41.1 cm femur and a 35.0 cm tibia with a mechanically neutral femur, restricting the sagittal misalignment to ±10° and the tibial component transverse rotation to ±5° results in $\widehat{\theta}_{t,cor}$ error of at most ±1°.

The forward model assumes that the surgeon articulates the knee, bringing the tibia parallel to the femur coronal plane (Fig. 7), prior to performing the specified joint line rotation maneuver. In practice it is difficult to determine when this parallel relationship is satisfied; furthermore, such alignment may not be possible in patients with an uncorrected flexion contracture. The effect of residual flexion stemming from flexion contracture, improper technique, or any other cause was assessed by injecting an offset into θ_{artic} in the forward model. As shown in Fig. 10, the tibia coronal angle estimate error associated with moderate (±10°) residual flexion falls within ±0.5° and is relatively insensitive to significant changes in the effective articulation radius.

4.3. Leg jig and cadaver evaluations

The left frame of Fig. 11 shows results from constrained leg jig testing in which we observed a highly linear coronal angle prediction, slightly deviating from unity slope, with very little inter-trial variation (maximum standard deviation 0.15°). The more realistic elevated leg jig simulation (Fig. 11, center) produced a trend line of nearly identical slope, but as expected, more variation was present between trials at each setting of the tibia coronal angle (maximum standard deviation 0.50°).

During the cadaver evaluation the -2° (varus) and 0° (neutral) tibia coronal angle configurations were associated with a 3° posterior slope, and the +2° (valgus) coronal angle configuration was associated with a 6° posterior slope. The results (Fig. 11, right) show a trend line through the mean estimates with slope very near unity and a static offset of 0.5°. Significant variation is present within each configuration (maximum

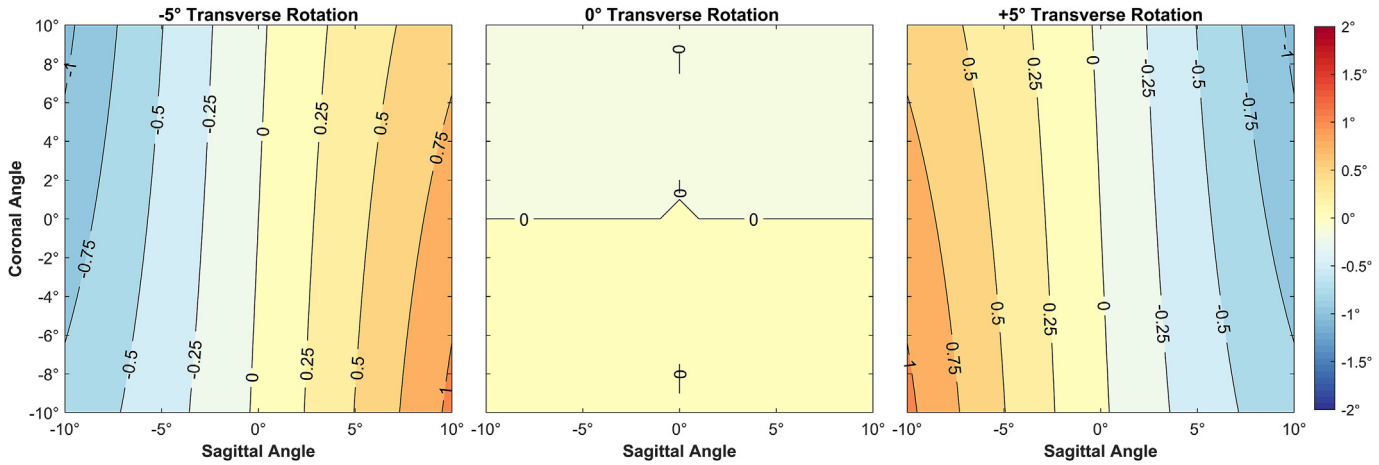

Fig. 9. Tibia coronal angle estimate error associated with sagittal and transverse plane misalignment was calculated using the forward model (Fig. 6). Error is not expected to exceed $\pm 1^\circ$ across a clinically relevant range of tibial coronal, sagittal, and transverse angles. These estimates assume a mechanically neutral femur, respective femur and tibia lengths of 41.1 cm and 35.0 cm, and an effective articulation radius of 31.75 mm.

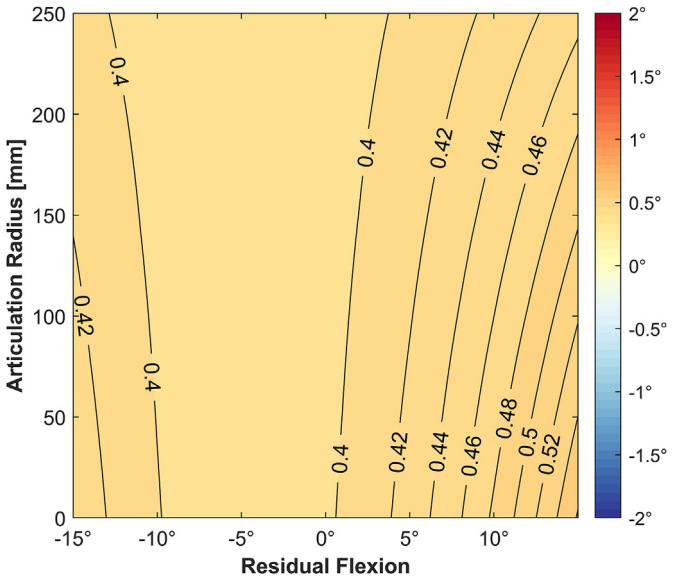

Fig. 10. Tibia coronal angle estimate error remains well below $\pm 1^\circ$ across a clinically-relevant range of effective articulation radii and residual flexion angles (e.g. from flexion contracture or misalignment during intraoperative manipulation) for nominal tibia coronal, sagittal, and transverse angles of $+5^\circ$, -5°, and $+5^\circ$, respectively. The tibia coronal angle estimate is relatively insensitive to the radius of articulation in this region.

standard deviation 0.82°), consistent with a mechanically unconstrained surgical environment.

5. Discussion

Our analysis of error in the proposed tibia coronal angle calculation (1) associated with measurement noise (Fig. 8) and out-of-plane misalignment (Figs. 9 and 10), along with bench-top testing and an initial cadaver study (Fig. 11), support the feasibility of gyroscope-based intraoperative evaluation of tibia alignment in the presence of $\pm 10^\circ$ sagittal and $\pm 5^\circ$ transverse deviations from neutral. Overall estimation accuracy on the order of $\pm 1^\circ$ approaches that of traditional surgical navigation, and shows promise for meeting or exceeding the $\pm 2^\circ$ accuracy reported for state-of-the-art accelerometer-based alignment systems [46,47].

The proposed method offers a number of advantages over similar portable systems. The gyroscope-based system is compatible with smoother, less-jerky intraoperative manipulations than systems that rely on generating substantial linear acceleration at the knee. As a post-resection alignment verification tool rather than a cutting guide positioning aid, the proposed system provides a more direct measure of component orientation taken from within the fully-assembled prosthetic. Given that the device housing is designed to mimic actual TKA bearing geometry, it is inherently compatible with specific implant systems and does not require any additional sterile instrumentation beyond the gyroscope-enabled insert and a display for readout. Finally, the error characteristics of the gyroscope-based $\widehat{\theta}_{t,cor}$ estimate can be readily determined as we describe herein to inform both system design and clinical implementation.

Further analysis and evaluation of this method will be required to better understand the bias observed during leg jig testing and reduce the estimate variability observed in the cadaver experiment. Future cadaver studies may require radiographic validation of the coronal and sagittal plane cut angles to serve as a more direct ground truth measurement than navigation, which is itself subject to error and variability [22,24–26].

As currently implemented, this method requires accurate knowledge of the femur coronal angle, taken with respect to the mechanical axis of the femur; however, similar IMU-based techniques may be employed to extract this information from intraoperative manipulation. If required, the coronal model developed herein can be integrated into an estimation scheme in which all IMU accelerometer and gyroscope data are assimilated, along with knowledge of the nominal manipulations and anatomical constraints, to simultaneously estimate the relevant femur and tibia alignment parameters. IMU data fusion is an evolving technology [43,55–57] that may enable accommodation of significant off-axis dynamic deviations in the intraoperative manipulation (an acknowledged limitation of the current method), but would also require a broader validation effort prior to clinical deployment due to the complexities and stochastic nature of state estimation.

Although beyond the scope of this work, it is interesting to observe that a similar form of (2) in which ω_y replaces ω_x can be used (with a factor of -1) to estimate the sagittal inclination of the proximal tibia resection plane. The resulting calculation is more sensitive to out-of-plane errors, but sagittal alignment (e.g. posterior slope) is typically less of a clinical concern as knee articulation accommodates even moderate variation.

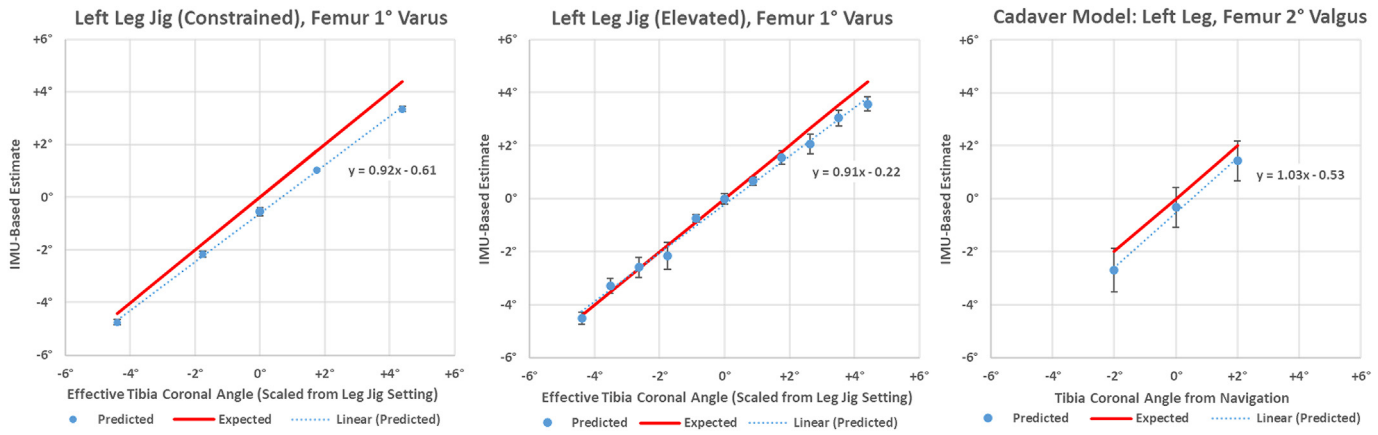

Fig. 11. Experimental estimates of tibia coronal angle from testing with the constrained leg jig (left), elevated leg jig (center), and cadaver model (right). Note that while relaxation of constraints leads to more variability in the resulting estimates, the trends in all cases approximate the expected slope of 1.0. Error bars are drawn at ±1 standard deviation.

6. Conclusion

Gyroscope-based estimation of the tibia coronal angle shows promise for clinical assessment of limb alignment during TKA surgery. We demonstrate sub-degree accuracy on average in mechanical simulations and similar performance, albeit with larger variability, in an initial cadaver study. Future work will be directed toward reducing this variability and the dependence on prior knowledge of the femur coronal angle.

Funding sources

This work was supported by OrthoSensor, Inc., Dania Beach, FL [grant number 20151001].

Declaration of competing interest

MWR was a founder and the Chief Medical of Officer OrthoSensor, Inc. (now part of Stryker Corp.). RMC and DWVC are named inventors on a related patent, but have assigned their rights and hold no future financial interests. DWVC receives academic research support as principal investigator from DePuy Synthes Joint Reconstruction, ConforMIS, RevBio, and TJO. See CRediT author statement for full detail.

Acknowledgments

The authors are grateful for experimental assistance from Daniel Lieffort. Contour color maps were generated with ColorBrewer [58].

References

[1] O'Keefe RJ, Chu CR, Jacobs JJ, Einhorn TA. Orthopaedic basic science : foundations of clinical practice. Rosemont: American Academy of Orthopaedic Surgeons; 2013.
[2] Bozic KJ, Kurtz SM, Lau E, Ong K, Chiu V, Vail TP, Rubash HE, Berry DJ. The epidemiology of revision total knee arthroplasty in the United States. Clin Orthop Relat Res 2010;468:45–51. https://doi.org/10.1007/s11999-009-0945-0.
[3] Lingard EA, Katz JN, Wright EA, Sledge CB, Kinemax Outcomes G. Predicting the outcome of total knee arthroplasty. J Bone Joint Surg Am 2004;86-A(10):2179–86. https://doi.org/10.2106/00004623-200410000-00008.
[4] Bourne RB, Chesworth BM, Davis AM, Mahomed NN, Charron KD. Patient satisfaction after total knee arthroplasty: who is satisfied and who is not? Clin Orthop Relat Res 2010;468(1):57–63. https://doi.org/10.1007/s11999-009-1119-9.
[5] Beswick AD, Wylde V, Gooberman-Hill R, Blom A, Dieppe P. What proportion of patients report long-term pain after total hip or knee replacement for osteoarthritis? A systematic review of prospective studies in unselected patients. BMJ Open 2012; 2(1):e000435. https://doi.org/10.1136/bmjopen-2011-000435.
[6] HCUP National Inpatient Sample (NIS). Healthcare cost and utilization Project (HCUP). Rockville, MD: Agency for Healthcare Research and Quality; 2012.
[7] Sloan M, Premkumar A, Sheth NP. Projected volume of primary total joint arthroplasty in the U.S., 2014 to 2030. J Bone Joint Surg Am 2018;100(17): 1455–60. https://doi.org/10.2106/JBJS.17.01617.
[8] Singh JA, Yu S, Chen L, Cleveland JD. Rates of total joint replacement in the United States: future projections to 2020-2040 using the national inpatient sample. J Rheumatol 2019;46(9):1134–40. https://doi.org/10.3899/jrheum.170990.
[9] Ethgen O, Bruyere O, Richy F, Dardennes C, Reginster JY. Health-related quality of life in total hip and total knee arthroplasty. A qualitative and systematic review of the literature. J Bone Joint Surg Am 2004;86-A(5):963–74. https://doi.org/10.2106/00004623-200405000-00012.
[10] Schwartz AM, Farley KX, Guild GN, Bradbury Jr TL. Projections and epidemiology of revision hip and knee arthroplasty in the United States to 2030. J Arthroplasty 2020;35(6S):S79–85. https://doi.org/10.1016/j.arth.2020.02.030.
[11] Waterson HB, Clement ND, Eyres KS, Mandalia VI, Toms AD. The early outcome of kinematic versus mechanical alignment in total knee arthroplasty: a prospective randomised control trial. Bone Joint J 2016;98-B(10):1360–8. https://doi.org/10.1302/0301-620X.98B10.36862.
[12] Schiraldi M, Bonzanini G, Chirillo D, de Tullio V. Mechanical and kinematic alignment in total knee arthroplasty. Ann Transl Med 2016;4(7):130. https://doi.org/10.21037/atm.2016.03.31.
[13] Insall JN, Binazzi R, Soudry M, Mestriner LA. Total knee arthroplasty. Clin Orthop Relat Res 1985;192:13–22. https://doi.org/10.1097/00003086-198501000-00003.
[14] Werner FW, Ayers DC, Maletsky LP, Rullkoetter PJ. The effect of valgus/varus malalignment on load distribution in total knee replacements. J Biomech 2005; 38(2):349–55. https://doi.org/10.1016/j.jbiomech.2004.02.024.
[15] Cherian JJ, Kapadia BH, Banerjee S, Jauregui JJ, Issa K, Mont MA. Mechanical, anatomical, and kinematic Axis in TKA: concepts and practical applications. Curr Rev Musculoskelet Med 2014;7(2):89–95. https://doi.org/10.1007/s12178-014-9218-y.
[16] Abdel MP, Oussedik S, Parratte S, Lustig S, Haddad FS. Coronal alignment in total knee replacement: historical review, contemporary analysis, and future direction. Bone Joint J 2014;96-B(7):857–62. https://doi.org/10.1302/0301-620X.96B7.33946.
[17] Lording T, Lustig S, Neyret P. Coronal alignment after total knee arthroplasty. EFORT Open Reviews 2016;1(1):12–7. https://doi.org/10.1302/2058-5241.1.000002.
[18] Jeffery R, Morris R, Denham R. Coronal alignment after total knee replacement. J Bone Joint Surg Br 1991;73-B(5):709–14. https://doi.org/10.1302/0301-620X.73B5.1894655.
[19] Fang DM, Ritter MA, Davis KE. Coronal alignment in total knee arthroplasty: just how important is it? J Arthroplasty 2009;24(6 Suppl):39–43. https://doi.org/10.1016/j.arth.2009.04.034.
[20] Davis JA, Hogan C, Dayton M. Postoperative coronal alignment after total knee arthroplasty: does tailoring the femoral valgus cut angle really matter? J Arthroplasty 2015;30(8):1444–8. https://doi.org/10.1016/j.arth.2015.03.013.
[21] Parratte S, Pagnano MW, Trousdale RT, Berry DJ. Effect of postoperative mechanical axis alignment on the fifteen-year survival of modern, cemented total knee replacements. J Bone Joint Surg Am 2010;92(12):2143–9. https://doi.org/10.2106/JBJS.I.01398.
[22] Haaker RG, Stockheim M, Kamp M, Proff G, Breitenfelder J, Ottersbach A. Computer-assisted navigation increases precision of component placement in total knee arthroplasty. Clin Orthop Relat Res 2005;433:152–9. https://doi.org/10.1097/01.blo.0000150564.31880.c4.
[23] Teter KE, Bregman D, Colwell Jr CW. Accuracy of intramedullary versus extramedullary tibial alignment cutting systems in total knee arthroplasty. Clin Orthop Relat Res 1995;321:106–10. https://doi.org/10.1097/00003086-199512000-00016.
[24] Martin A, Wohlgenannt O, Prenn M, Oelsch C, von Strempel A. Imageless navigation for TKA increases implantation accuracy. Clin Orthop Relat Res 2007; 460:178–84. https://doi.org/10.1097/BLO.0b013e31804ea45f.

[25] Yau WP, Chiu KY, Zuo JL, Tang WM, Ng TP. Computer navigation did not improve alignment in a lower-volume total knee practice. Clin Orthop Relat Res 2008; 466(4):935–45. https://doi.org/10.1007/s11999-008-0144-4.
[26] Novak EJ, Silverstein MD, Bozic KJ. The cost-effectiveness of computer-assisted navigation in total knee arthroplasty. J Bone Joint Surg Am 2007;89(11):2389–97. https://doi.org/10.2106/jbjs.f.01109.
[27] Rhee SJ, Park SH, Cho HM, Suh JT. Comparison of precision between optical and electromagnetic navigation systems in total knee arthroplasty. Knee Surg Relat Res 2014;26(4):214–21. https://doi.org/10.5792/ksrr.2014.26.4.214.
[28] Sicat CS, Chow JC, Kaper B, Mitra R, Xie J, Schwarzkopf R. Component placement accuracy in two generations of handheld robotics-assisted knee arthroplasty. Arch Orthop Trauma Surg 2021;141(12):2059–67. https://doi.org/10.1007/s00402-021-04040-6.
[29] Bathis H, Perlick L, Tingart M, Luring C, Zurakowski D, Grifka J. Alignment in total knee arthroplasty. A comparison of computer-assisted surgery with the conventional technique. J Bone Joint Surg Br 2004;86(5):682–7. https://doi.org/10.1302/0301-620x.86b5.14927.
[30] Choong PF, Dowsey MM, Stoney JD. Does accurate anatomical alignment result in better function and quality of life? Comparing conventional and computer-assisted total knee arthroplasty. J Arthroplasty 2009;24(4):560–9. https://doi.org/10.1016/j.arth.2008.02.018.
[31] Anderson KC, Buehler KC, Markel DC. Computer assisted navigation in total knee arthroplasty: comparison with conventional methods. J Arthroplasty 2005;20(7 Suppl 3):132–8. https://doi.org/10.1016/j.arth.2005.05.009.
[32] Molli RG, Anderson KC, Buehler KC, Markel DC. Computer-assisted navigation software advancements improve the accuracy of total knee arthroplasty. J Arthroplasty 2011;26(3):432–8. https://doi.org/10.1016/j.arth.2010.01.002.
[33] Sparmann M, Wolke B, Czupalla H, Banzer D, Zink A. Positioning of total knee arthroplasty with and without navigation support. A prospective, randomised study. J Bone Joint Surg Br 2003;85(6):830–5. https://doi.org/10.1302/0301-620X.85B6.13722.
[34] Mason JB, Fehring TK, Estok R, Banel D, Fahrbach K. Meta-analysis of alignment outcomes in computer-assisted total knee arthroplasty surgery. J Arthroplasty 2007; 22(8):1097–106. https://doi.org/10.1016/j.arth.2007.08.001.
[35] Hetaimish BM, Khan MM, Simunovic N, Al-Harbi HH, Bhandari M, Zalzal PK. Meta-analysis of navigation vs conventional total knee arthroplasty. J Arthroplasty 2012; 27(6):1177–82. https://doi.org/10.1016/j.arth.2011.12.028.
[36] de Steiger RN, Liu YL, Graves SE. Computer navigation for total knee arthroplasty reduces revision rate for patients less than sixty-five years of age. J Bone Joint Surg Am 2015;97(8):635–42. https://doi.org/10.2106/jbjs.m.01496.
[37] Decking R, Markmann Y, Fuchs J, Puhl W, Scharf HP. Leg axis after computer-navigated total knee arthroplasty: a prospective randomized trial comparing computer-navigated and manual implantation. J Arthroplasty 2005;20(3):282–8. https://doi.org/10.1016/j.arth.2004.09.047.
[38] Sires JD, Wilson CJ. CT validation of intraoperative implant position and knee alignment as determined by the MAKO total knee arthroplasty system. J Knee Surg 2021;34(10):1133–7. https://doi.org/10.1055/s-0040-1701447.
[39] Vermue H, Luyckx T, Winnock de Grave P, Ryckaert A, Cools AS, Himpe N, Victor J. Robot-assisted total knee arthroplasty is associated with a learning curve for surgical time but not for component alignment, limb alignment and gap balancing. Knee Surg Sports Traumatol Arthrosc 2020. https://doi.org/10.1007/s00167-020-06341-6.
[40] Sousa PL, Sculco PK, Mayman DJ, Jerabek SA, Ast MP, Chalmers BP. Robots in the operating room during hip and knee arthroplasty. Curr Rev Musculoskelet Med 2020;13(3):309–17. https://doi.org/10.1007/s12178-020-09625-z.
[41] Takeda R, Tadano S, Natorigawa A, Todoh M, Yoshinari S. Gait posture estimation using wearable acceleration and gyro sensors. J Biomech 2009;42(15):2486–94. https://doi.org/10.1016/j.jbiomech.2009.07.016.
[42] Ma J, Kharboutly H, Benali A, Amar FB, Bouzit M. Design of omnidirectional mobile platform for balance analysis. IEEE ASME Trans Mechatron 2014;19(6):1872–81. https://doi.org/10.1109/TMECH.2014.2309484.
[43] Weygers I, Kok M, Vroey HD, Verbeerst T, Versteyhe M, Hallez H, Claeys K. Drift-free inertial sensor-based joint kinematics for long-term arbitrary movements. IEEE Sensor J 2020;20(14):7969–79. https://doi.org/10.1109/JSEN.2020.2982459.
[44] Chapman RM, Moschetti WE, Van Citters DW. Stance and swing phase knee flexion recover at different rates following total knee arthroplasty: an inertial measurement unit study. J Biomech 2019;84:129–37. https://doi.org/10.1016/j.jbiomech.2018.12.027.
[45] Bugbee WD, Kermanshahi AY, Munro MM, McCauley JC, Copp SN. Accuracy of a hand-held surgical navigation system for tibial resection in total knee arthroplasty. Knee 2014;21(6):1225–8. https://doi.org/10.1016/j.knee.2014.09.006.
[46] Nam D, Cody EA, Nguyen JT, Figgie MP, Mayman DJ. Extramedullary guides versus portable, accelerometer-based navigation for tibial alignment in total knee arthroplasty: a randomized, controlled trial: winner of the 2013 HAP Paul award. J Arthroplasty 2014;29(2):288–94. https://doi.org/10.1016/j.arth.2013.06.006.
[47] Nam D, Weeks KD, Reinhardt KR, Nawabi DH, Cross MB, Mayman DJ. Accelerometer-based, portable navigation vs imageless, large-console computer-assisted navigation in total knee arthroplasty: a comparison of radiographic results. J Arthroplasty 2013;28(2):255–61. https://doi.org/10.1016/j.arth.2012.04.023.
[48] Nam D, Jerabek SA, Haughom B, Cross MB, Reinhardt KR, Mayman DJ. Radiographic analysis of a hand-held surgical navigation system for tibial resection in total knee arthroplasty. J Arthroplasty 2011;26(8):1527–33. https://doi.org/10.1016/j.arth.2011.01.012.
[49] Desseaux A, Graf P, Dubrana F, Marino R, Clave A. Radiographic outcomes in the coronal plane with iASSIST versus optical navigation for total knee arthroplasty: a preliminary case-control study. Orthop Traumatol Surg Res 2016;102(3):363–8. https://doi.org/10.1016/j.otsr.2016.01.018.
[50] Scuderi GR, Fallaha M, Masse V, Lavigne P, Amiot LP, Berthiaume MJ. Total knee arthroplasty with a novel navigation system within the surgical field. Orthop Clin N Am 2014;45(2):167–73. https://doi.org/10.1016/j.ocl.2013.11.002.
[51] Suda Y, Takayama K, Ishida K, Hayashi S, Hashimoto S, Niikura T, Matsushita T, Kuroda R, Matsumoto T. Improved implant alignment accuracy with an accelerometer-based portable navigation system in medial unicompartmental knee arthroplasty. Knee Surg Sports Traumatol Arthrosc 2020;28(9):2917–23. https://doi.org/10.1007/s00167-019-05669-y.
[52] Gharaibeh MA, Solayar GN, Harris IA, Chen DB, MacDessi SJ. Accelerometer-based, portable navigation (KneeAlign) vs conventional instrumentation for total knee arthroplasty: a prospective randomized comparative trial. J Arthroplasty 2017; 32(3):777–82. https://doi.org/10.1016/j.arth.2016.08.025.
[53] Reed SC, Gollish J. The accuracy of femoral intramedullary guides in total knee arthroplasty. J Arthroplasty 1997;12(6):677–82. https://doi.org/10.1016/s0883-5403(97)90141-8.
[54] Grood ES, Suntay WJ. A joint coordinate system for the clinical description of three-dimensional motions: application to the knee. J Biomech Eng 1983;105(2):136–44. https://doi.org/10.1115/1.3138397.
[55] Madgwick SOH, Wilson S, Turk R, Burridge J, Kapatos C, Vaidyanathan R. An extended complementary filter for full-body MARG orientation estimation. IEEE ASME Trans Mechatron 2020;25(4):2054–64. https://doi.org/10.1109/TMECH.2020.2992296.
[56] Poulose A, Eyobu OS, Han DS. An indoor position-estimation algorithm using smartphone IMU sensor data. IEEE Access 2019;7:11165–77. https://doi.org/10.1109/ACCESS.2019.2891942.
[57] Vihonen J, Honkakorpi J, Tuominen J, Mattila J, Visa A. Linear accelerometers and rate gyros for rotary joint angle estimation of heavy-duty mobile manipulators using forward kinematic modeling. IEEE ASME Trans Mechatron 2016;21(3):1765–74. https://doi.org/10.1109/TMECH.2016.2544352.
[58] Harrower M, Brewer CA. ColorBrewer.org: an online tool for selecting colour schemes for maps. Cartogr J 2003;40(1):27–37. https://doi.org/10.1179/000870403235002042.